

LETTER TO THE JOURNAL

Targeting ferroptosis resistance resensitizes metastatic HR⁺HER2⁻ breast cancer cells to palbociclib-hormone therapy

Metastatic hormone receptor-positive (HR⁺), human epidermal growth factor receptor 2-negative (HER2⁻) breast cancer often develops resistance to first-line treatment, typically combining cyclin-dependent kinase 4 and 6 inhibitors (CDK4/6i) with hormone therapy (HT) [1, 2]. After an initial response, most patients become resistant, and compensatory mechanisms are not fully uncovered [3]. To address this, we analyzed HR⁺ resistant CAMA1 and T47D cells using whole-exome and RNA sequencing, supplemented by proteomics and target validation with human samples. Additionally, we conducted combination therapy trials using xenografts and patient-derived xenografts (PDXs). Detailed study designs and methods are provided in the [Supplementary file](#).

In a cohort of 27 patients with metastatic breast cancer, we observed reduced progression-free survival in second- and third-line therapies following progression post palbociclib-HT treatment (Supplementary Figure S1A and Supplementary Table S1). Resistant tumors showed reduced estrogen receptor alpha (ER α) and progesterone receptor (PR) and increased proliferation rates (Supplementary Figure S1B-D). CAMA1 and T47D cells, treated with palbociclib and fulvestrant (PF) for 2 years, developed resistance (CAMA1-PFR and T47D-PFR) confirmed by proliferation assays and elevated half-maximal inhibitory concentrations. Resistant cells exhibited reduced levels of ER α and retinoblastoma protein (Supplementary Figure S2). Exome analysis revealed no drug resistance-related mutations (Supplementary Tables S2-S3), suggesting non-genetic factors.

Abbreviations: CD36, cluster of differentiation 36; CDK4/6, cyclin-dependent kinase 4 and 6; ER α , estrogen receptor alpha; FABP6, fatty acid binding protein-6; FABP7, fatty acid binding protein-7; GPX4, glutathione peroxidase 4; GSH, reduced glutathione; HER2, epidermal growth factor receptor 2; HNE, hydroxynonenal; HR, hormone receptor; HT, hormone therapy; PDX, patient-derived xenografts; PPAR γ , proliferator-activated receptor gamma; ROS, reactive oxygen species.

RNA sequencing of T47D cells treated with DMSO or PF for 20 days and T47D-PFR cells revealed 1,172 upregulated genes and 824 downregulated genes in the resistant cells (Supplementary Figure S3A). Gene set enrichment analysis indicated increased fatty acid localization (Supplementary Figure S3B), with a heatmap showing elevated fatty acid uptake and metabolism-related genes, such as fatty acid binding protein-6 (FABP6), FABP7, cluster of differentiation-36 (CD36), and proteasome proliferator-activated receptor-gamma (PPAR γ) in T47D-PFR cells (Figure 1A). Lipid droplets accumulated in PF-treated parental and PF-resistant T47D and CAMA1 cells (Figure 1B and Supplementary Figure S3C). FABP6 levels were elevated in PF-treated parental and PF-resistant cells, with CD36 overexpression unique to T47D-PFR cells at both protein and mRNA levels (Figure 1C and Supplementary Figure S3D-E), suggesting that lipid uptake might be an adaptive response to oxidative stress [4, 5]. This was supported by elevated reactive oxygen species (ROS) levels in PF-treated parental cells (Figure 1D). Furthermore, proteomic analysis in human biopsies revealed a functional network of 11 oxidative stress-triggered proteasomes (Supplementary Figure S4A and Supplementary Tables S4-S5) as indicators of oxidative stress [6]. Immunohistochemistry validated increased proteasome subunit alpha type-7 (PSMA7) in resistant biopsies (Supplementary Figure S4B).

We investigated whether cell survival is affected by ferroptosis—a type of non-apoptotic cell death linked to lipid peroxidation. GPX4 protein, the main protector against ferroptosis, was overexpressed in parental cells after PF treatment and in PF-resistant cells, even after drug wash-out, with no changes in mRNA levels (Figure 1E and Supplementary Figure S5A-C). Silencing GPX4 expression reduced cell proliferation in parental and PF-resistant cells (Supplementary Figure S5D-F), indicating their reliance on GPX4. GPX4 overexpression was also observed in resistant human tumors (Figure 1F).

This is an open access article under the terms of the [Creative Commons Attribution-NonCommercial-NoDerivs](#) License, which permits use and distribution in any medium, provided the original work is properly cited, the use is non-commercial and no modifications or adaptations are made.

© 2024 The Author(s). *Cancer Communications* published by John Wiley & Sons Australia, Ltd on behalf of Sun Yat-sen University Cancer Center.

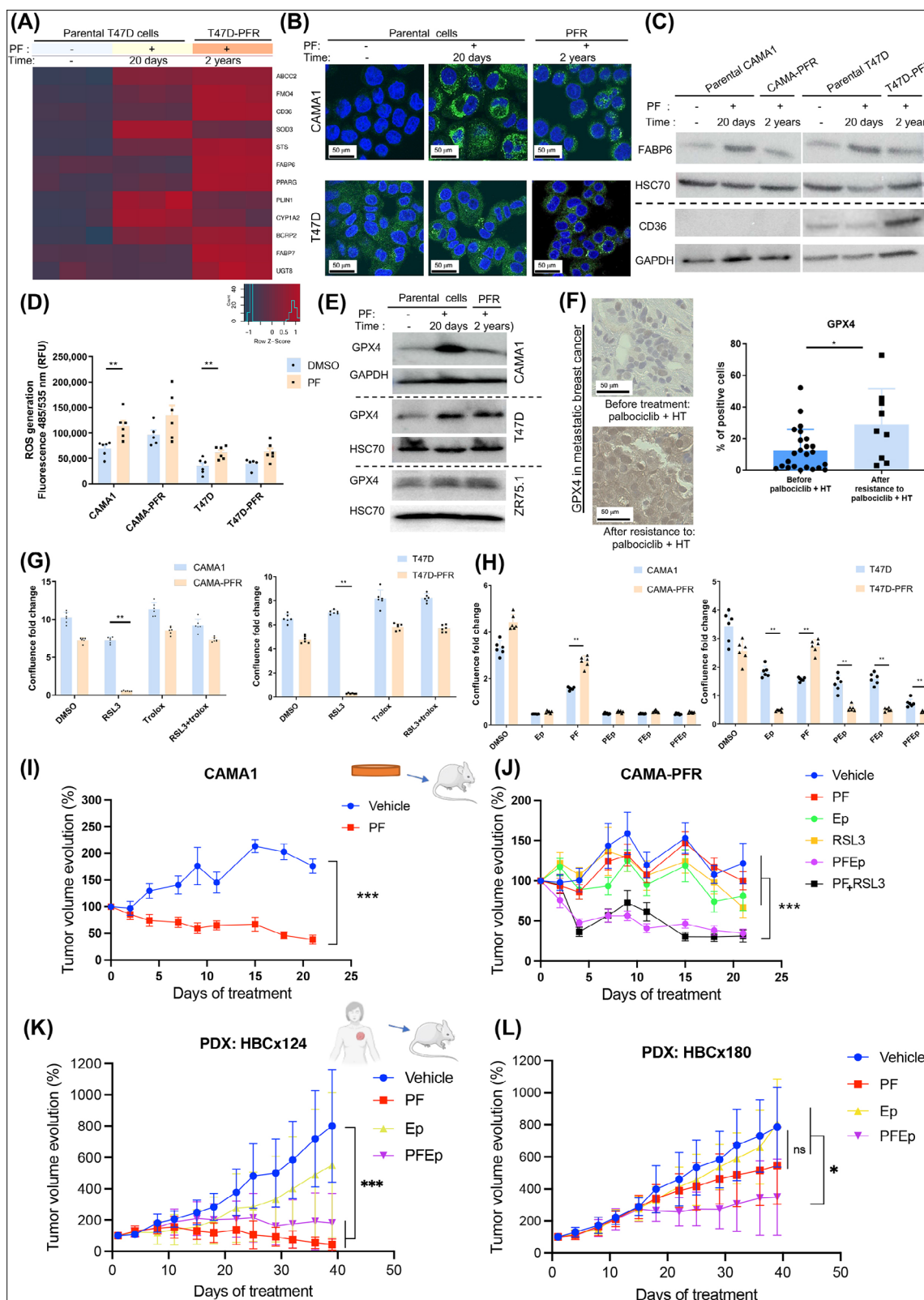


FIGURE 1 Ferroptosis inducers overcome resistance of HR⁺HER2⁻ breast cancer cells to palbociclib-hormone therapy. (A) Heatmap of upregulated genes (red) or downregulated genes (blue) during the treatment of T47D cells with PF combination for 20 days, and in PF-resistant cells (T47D-PFR) after continuous PF treatment for 2 years, compared to parental T47D cells treated with vehicle (DMSO). All represented genes had a P value < 0.05 . (B) Lipid droplet detection by BODIPY 493/503 staining in parental CAMA1 and T47D cells after treatment with the PF combination for 20 days, and in CAMA1-PFR and T47D-PFR cells after continuous PF treatment for 2 years. DAPI staining was used to visualize the nuclei. (C) Western blot analysis of FABP6 and CD36 in parental CAMA1 and T47D cells after treatment with the PF combination for 20 days, and in CAMA1-PFR and T47D-PFR cells after continuous PF treatment for 2 years. (D) Measurement of

Cells were treated with the GPX4 inhibitor RAS-selective lethal 3 (RSL3) and the antioxidant Trolox for 6 days. CAMA1 and T47D cells were insensitive to RSL3, whereas CAMA1-PFR and T47D-PFR cells showed high sensitivity to RSL3 (Figure 1G). Trolox reversed RSL3's effect in both cell lines (Figure 1G), highlighting the role of GPX4 in PF-resistant cell proliferation. Due to unverified safety of RSL3, we used eprenetapopt (Ep), a p53 activator and GSH depletory [7] proven safe in hematological cancer patients [8]. In vitro, CAMA1 and CAMA1-PFR cells were sensitive to Ep, while T47D cells were insensitive; T47D-PFR showed higher sensitivity (Figure 1H).

To investigate the effect of pharmacologically induced ferroptosis on the palbociclib-fulvestrant response in vivo, we used nude mice implanted with estrogen pellets. Due to its low pharmacokinetics in mouse plasma [9], RSL3 was administered via intratumoral injection. Mice were treated with vehicle, PF, Ep, RSL3, a combination of palbociclib-fulvestrant and eprenetapopt (PFEP), or a combination of palbociclib-fulvestrant and RSL3 (PF-RSL3). PF effectively inhibited the growth of the CAMA1 xenografts, while CAMA1-PFR tumors were insensitive (Figure 1I and J). RSL3 alone did not affect CAMA1-PFR tumor growth, whereas PF-RSL3 demonstrated a strong antitumor effect (Figure 1J), suggesting that RSL3 sensitizes CAMA1-PFR cells to PF, or vice versa. Similarly, Ep alone did not inhibit CAMA1-PFR tumor growth, but its combination with PF completely abolished tumor growth (Figure 1J).

To evaluate treatment effects on proliferation and cell death, we assessed Ki67, caspase-3 and hydroxynonenal (HNE) in tumors by immunohistochemistry. Parental CAMA1 tumors treated with PF showed a significant decrease in Ki67, with no effect on caspase-3, while CAMA1-PFR tumors exhibited no significant changes in either marker after treatment with PF, PFEP, or PF-RSL3 (Supplementary Figure S6A-D). HNE labeling revealed no difference between PF- and vehicle-treated CAMA1 tumors (Supplementary Figure S6E), but HNE increased moderately in CAMA1-PFR tumors treated with RSL3 and significantly with PFEP or PF-RSL3 (Supplementary Figure S6F), indicating potential cell death by ferroptosis. No treatments affected CD36 expression in either tumor type, although CAMA1-PFR xenografts showed significantly increased basal expression compared to human biopsies (Supplementary Figure S6G-J).

To strengthen the translational impact of our findings, we used patient-derived xenografts (PDXs) from HR⁺HER2⁻ breast cancer patients without p53 mutations (Supplementary Figure S7A) [10]. Consistent with human samples, GPX4 protein was upregulated in the palbociclib-HT-resistant PDX model (HBCx-180) compared to the palbociclib-HT-naïve PDX model (HBCx-124) (Supplementary Figure S7B). While GPX4 mRNA levels were unaffected in resistant cells, its expression was significantly higher in HBCx-180 (Supplementary Figure S7C), suggesting specific transcriptional/translational

ROS levels by DCFDA ROS assay in parental CAMA1 and T47D cells and in CAMA1-PFR and T47D-PFR cells treated for 5 days with DMSO or PF. Continuous PF treatment for resistant cells was discontinued 3 days prior to the assay. (E) Western blot analysis of GPX4 in parental CAMA1, T47D and ZR75.1 cells after treatment with PF combination for 20 days and in CAMA1-PFR, T47D-PFR and ZR75.1-PFR cells after continuous PF treatment for 2 years. (F) Immunohistochemistry analysis (images) and quantification (bar chart) of GPX4-positive cells in biopsies of patients taken before treatment with palbociclib-HT or after resistance (**P* < 0.05). (G) Assessment of cell proliferation according to the fold change in confluence in parental and PF-resistant CAMA1 and T47D cells treated with DMSO, the ferroptosis inducer RSL3 (1 μmol/L), the ferroptosis inhibitor Trolox (10 μmol/L), or a combination of both for 7 days. Continuous PF treatment for resistant cells was discontinued 3 days prior to the assay. (H) Assessment of cell proliferation according to the fold change in confluence in parental and PF-resistant CAMA1 and T47D cells treated with different combinations of DMSO, palbociclib (P) (0.3 μmol/L), fulvestrant (F) (30 nmol/L), or eprenetapopt (Ep) (25 μmol/L) for 7 days. Continuous PF treatment for resistant cells was discontinued 3 days prior to the assay. (I, J) Tumor growth curves of parental CAMA1 (6 mice per group) (I) and CAMA1-PFR (8 mice per group) (J) xenografts treated with different combinations of palbociclib (P) 75 mg/kg daily, fulvestrant (F) 50 mg/kg once a week, and eprenetapopt (Ep) 150 mg/kg, 2 times/day or RSL3 100 mg/kg by intratumoral injection every two days for two weeks (****P* < 0.001). (K) Growth curves of palbociclib-HT-naïve HBCx-124 PDXs (5 mice per group) treated with different combinations of palbociclib (P) 75 mg/kg daily, fulvestrant (F) 50 mg/kg once a week, and eprenetapopt (Ep) 150 mg/kg, 2 times/day (****P* < 0.001). (L) Growth curves of palbociclib-HT-resistant HBCx-180 PDXs (8 mice per group) treated with different combinations of palbociclib (P) 75 mg/kg daily, fulvestrant (F) 50 mg/kg once a week, and eprenetapopt (Ep) 150 mg/kg, 2 times/day. The difference between the measured tumor volumes was significant between the "vehicle" group and the eprenetapopt + fulvestrant + palbociclib (FPE) group from Day 25 until the end of the experiment (*P* < 0.05). Tumor evolution formula is $(V_f - V_0 / V_0) \times 100\%$, where *V*₀ is the initial volume and *V*_f is the final volume measured at each time point.

Abbreviations: CD36, cluster of differentiation 36; DAPI, 4',6-diamidino-2-phenylindole; DCFDA, 2',7'-Dichlorofluorescein Diacetate; DMSO, dimethyl sulfoxide; Ep, eprenetapopt; FABP6, fatty acid binding protein 6; GPX4, Glutathione peroxidase 4; HR⁺HER2⁻, hormone receptor positive and human epidermal growth factor receptor-2 negative; HT, hormone therapy; PDX, patient-derived xenograft; PF, palbociclib-fulvestrant; PF RSL3, palbociclib-fulvestrant-RSL3; PFE, palbociclib-fulvestrant-eprenetapopt; ROS, reactive oxygen species, RSL3, ras-selective lethal small molecule 3; Trolox, 6-hydroxy-2,5,7,8-tetramethylchroman-2-carboxylic acid.

regulation differing between in vitro and in vivo contexts. In the HBCx-124 model, all the tumors ($n = 5$) responded well to PF, with no added benefit from Ep (PFEP), although a partial response to Ep monotherapy was observed (Figure 1K). Conversely, the HBCx-180 model showed no significant response to PF or Ep, with significant differences in tumor volumes between PFEP and vehicle and Ep groups from Day 25 onward ($P < 0.05$) (Figure 1L). These results confirm that adding Ep to PF in PF-resistant tumors produces a strong antitumor effect. Ki67 labeling decreased with PF in the HBCx-124 PDX but not in the HBCx-180 PDX (Supplementary Figure S8A–B). Aside from reduction in caspase-3 labeling in the HBCx-124 treated with PF, no significant changes were observed with Ep or PFEP, and none of the treatment conditions affected HBCx-180 (Supplementary Figure S8C–D), indicating that proliferation and apoptosis are not affected in HBCx-180. HNE labeling suggested that PF promoted ferroptosis in HBCx-124, while only tumors treated with PFEP in HBCx-180 exhibited significant HNE increase compared to vehicle (Supplementary Figure S8E–F). PF slightly increased HNE in HBCx-124 without significance but the only vulnerability of HBCx-180 is attributed to ferroptosis induced with PFEP. The p53-dependent antitumor effect of epremetastat was excluded, as p53 expression was similar in parental and PF-resistant cells and in PDXs, while slightly elevated in resistant human tumors (Supplementary Figure S9). Finally, the addition of Ep or RSL3 to PF did not induce significant renal, hepatic, or hematological toxicity in mice (Supplementary Figure S10).

In conclusion, HR⁺HER2[−] tumors resistant to palbociclib-HT are vulnerable to ferroptosis inducers, highlighting the potential of collateral drug sensitivity and the promise of developing pro-ferroptosis agents for treating drug-resistant metastatic breast cancer (Supplementary Figure S11).

AUTHOR CONTRIBUTIONS

Conception and design: CP and NES. Development of methodology: CP, LMR, NES. Acquisition of data: CP, LMR, RT, CW, RJ, AR, JC, CJ, SG, SB, AD, PD, LM and EM. Analysis and interpretation of data (e.g., statistical analysis, biostatistics): CP, LMR, DB, GM, RT, CJ and NES. Writing, review, and/or revision of the manuscript: CP, GJ, AN and NES. Study supervision: GJ and NES.

ACKNOWLEDGMENTS

The authors thank the Cell Imaging Core Facility of the GIGA institute for Incucyte and fluorescence microscopy experiments; Isabelle Dasoul, Emilie Feyereisen, Erika Konradowski and Nathalie Lefin for their technical support; Maud Piron for enrolling the cohort of patients; and Hélène Schroeder for correcting the file sent to the human ethics committee and the Biobank of Liège University for

providing human samples. The authors also thank Latifa Karim and Manon Deckers from the GIGA Sequencing Platform (ULiège, Belgium) for their help and advice; Erik Maquoi for image acquisition with Nanolive and Louis Baudin (Animascience, Liège, Belgium) for the graphical abstract.

CONFLICTS OF INTEREST STATEMENT

The authors declare no competing interest except for Dr. Guy Jerusalem, who declares receiving grant support, paid to his institution, advisory board fees, lecture fees, travel support, and writing assistance from Novartis, Roche, and Pfizer. Disclosure is provided with the full text of this article. No other potential conflicts of interest relevant to this article were reported.

FUNDING INFORMATION

This work was supported by grants from the National Fund for Scientific Research (NFSR-FNRS) Belgium (NES: PDR T.023020; CDR J.0178.22); the credit sectorial of the University of Liege (NES: FSR-S-SS-22/61; FSR-S-SS-22/64); and the Foundation Contre le Cancer, Belgium (NES and AN: FCC-2022-181).

DATA AVAILABILITY STATEMENT

RNA sequencing data were deposited in the GEO-NCBI depository with the accession number: GSE270021 Exome sequencing data were registered in the BioProject database with the identification number: PRJNA1027140 Proteomic data were deposited in PRIDE with accession number: PXD053296. The data that support the findings of this study are available from the corresponding author upon reasonable request.

ETHICAL APPROVAL AND CONSENT TO PARTICIPATE

A protocol was approved by the institutional Ethics Committee of the University Hospital of Liege (Liege, Belgium; file#2018/312) for the use of human samples in this study, and the ethical guidelines of the Declaration of Helsinki were followed. The ethical committee has authorized on May 15, 2019, to retrospectively use biopsies stored in the biobank of the University of Liège and anonymized clinical data associated with these biopsies. The committee noted that this non-interventional use has no impact on patients and is not within the scope of the law of May 7, 2004, on experiments on human beings and thus did not require informed consents. For the animal study, all procedures were performed according to the Federation of European Laboratory Animal Sciences Associations (FELASA) within the accredited GIGA animal facility (University of Liege, Liege, Belgium) (project authorization no. 2078). PDX experiments were performed at the Institute of Curie, in accordance with institutional

guidelines and the rules of the French Ethics Committee (project authorization no. 02163.02).

Charles Pottier^{1,2}
Laetitia Montero-Ruiz^{1,3}
Robin Jehay¹
Coline Wery¹
Dominique Baiwir⁴ 
Gabriel Mazzucchelli⁴
Sophie Bekisz⁵
Romain Thissen⁶
Claire Josse⁶
Andrée Rorive²
Stéphanie Gofflot⁷
Ahmed Dahmani⁸
Ludivine Morisset⁸
Joëlle Collignon²
Philippe Delvenne⁹
Elisabetta Marangoni⁸
Agnès Noël³
Guy Jerusalem²
Nor Eddine Sounni¹ 

¹*Cancer Metabolism and Tumor Microenvironment Group, Interdisciplinary Group for Applied Genoproteomics (GIGA), University of Liège, Liège, Belgium*

²*Medical Oncology Department, University Hospital of Liège, Liège, Belgium*

³*Laboratory of Tumor and Development Biology, Interdisciplinary Group for Applied Genoproteomics (GIGA) Appliquée, University of Liège, Liège, Belgium*

⁴*Proteomics Facility, Interdisciplinary Group for Applied Genoproteomics (GIGA), University of Liège, Liège, Belgium*

⁵*Biomechanics Research Unit, In silico Medicine, Interdisciplinary Group for Applied Genoproteomics (GIGA), University of Liège, Liège, Belgium*

⁶*Human Genetics Department, Interdisciplinary Group for Applied Genoproteomics (GIGA), University of Liège, Liège, Belgium*

⁷*Biobank of the University Hospital of Liège, University of Liège, Liège, Belgium*

⁸*Laboratory of Preclinical Investigation, Translational Research Department, Institut Curie, Paris, France*


⁹*Anatomie et cytologie pathologiques, University Hospital of Liège, Liège, Belgium*


Correspondence

Nor Eddine Sounni, Cancer Metabolism and Tumor Microenvironment Group, GIGA-Cancer, University of Liège, Avenue Hippocrate 13, B23, Sart Tilman, Liège 4000, Belgium.

Email: nesounni@uliege.be

ORCID

Dominique Baiwir  <https://orcid.org/0000-0002-1622-0118>

Nor Eddine Sounni  <https://orcid.org/0000-0001-9962-9236>

REFERENCES

1. Cristofanilli M, Turner NC, Bondarenko I, Ro J, Im SA, Masuda N, et al. Fulvestrant plus palbociclib versus fulvestrant plus placebo for treatment of hormone-receptor-positive, HER2-negative metastatic breast cancer that progressed on previous endocrine therapy (PALOMA-3): final analysis of the multicentre, double-blind, phase 3 randomised controlled trial. *Lancet Oncol.* 2016;17(4):425–439.
2. O'leary B, Cutts RJ, Liu Y, Hrebien S, Huang X, Fenwick K, et al. The Genetic Landscape and Clonal Evolution of Breast Cancer Resistance to Palbociclib plus Fulvestrant in the PALOMA-3 Trial. *Cancer Discov.* 2018;8(11):1390–1403.
3. Asghar US, Kanani R, Roylance R, Mittnacht S. Systematic Review of Molecular Biomarkers Predictive of Resistance to CDK4/6 Inhibition in Metastatic Breast Cancer. *JCO Precis Oncol.* 2022;6(6):e2100002.
4. Cadenas C, Vosbeck S, Edlund K, Grgas K, Madjar K, Hellwig B, et al. LIPG-promoted lipid storage mediates adaptation to oxidative stress in breast cancer. *Int J Cancer.* 2019;145(4):901–915.
5. Luis G, Godfroid A, Nishiumi S, Cimino J, Blacher S, Maquoi E, et al. Tumor resistance to ferroptosis driven by Stearoyl-CoA Desaturase-1 (SCD1) in cancer cells and Fatty Acid Binding Protein-4 (FABP4) in tumor microenvironment promote tumor recurrence. *Redox Biol.* 2021;43:102006.
6. Aiken CT, Kaake RM, Wang X, Huang L. Oxidative Stress-Mediated Regulation of Proteasome Complexes. *Mol Cell Proteomics.* 2011;10(5):R110.
7. Fujihara KM, Zhang BZ, Jackson TD, Ogunkola MO, Nijagal B, Milne JV, et al. Eprenetapopt triggers ferroptosis, inhibits NFS1 cysteine desulfurase, and synergizes with serine and glycine dietary restriction. *Sci Adv [Internet].* 2022;8(37):eabm9427.
8. Sallman DA, DeZern AE, Garcia-Manero G, Steensma DP, Roboz GJ, Sekeres MA, et al. Eprenetapopt (APR-246) and Azacitidine in TP53 -Mutant Myelodysplastic Syndromes. *J Clin Oncol.* 2021;39(14):1584–1594.
9. Randolph JT, O'Connor MJ, Han F, Hutchins CW, Siu YA, Cho M, et al. Discovery of a Potent Chloroacetamide GPX4 Inhibitor with Bioavailability to Enable Target Engagement in Mice, a Potential Tool Compound for Inducing Ferroptosis In Vivo. *J Med Chem.* 2023;66(6):3852–3865.
10. El-Botty R, Morriset L, Montaudon E, Tariq Z, Schnitzler A, Bacci M, et al. Oxidative phosphorylation is a metabolic vulnerability of endocrine therapy and palbociclib resistant metastatic breast cancers. *Nat Commun.* 2023;14(1):4221.

SUPPORTING INFORMATION

Additional supporting information can be found online in the Supporting Information section at the end of this article.